39th AIAA Thermophysics Conference, 25-28 June 2007, Miami, FL

One-Dimensional Ablation with Pyrolysis Gas Flow Using a Full Newton's Method and Finite Control Volume Procedure

A. J. Amar*

Sandia National Laboratories,†Albuquerque, New Mexico, 87185-0825

North Carolina State University, Raleigh, North Carolina, 27695-7910

B. F. Blackwell‡

Blackwell Consulting, Corrales, New Mexico, 87048

J. R. Edwards§

North Carolina State University, Raleigh, North Carolina, 27695-7910

The development and verification of a one-dimensional material thermal response code with ablation is presented. The implicit time integrator, control volume finite element spatial discretization, and Newton's method for nonlinear iteration on the entire system of residual equations have been implemented and verified for the thermochemical ablation of internally decomposing materials. This study is a continuation of the work presented in "One-Dimensional Ablation with Pyrolysis Gas Flow Using a Full Newton's Method and Finite Control Volume Procedure" (AIAA-2006-2910), which described the derivation, implementation, and verification of the constant density solid energy equation terms and boundary conditions. The present study extends the model to decomposing materials including decomposition kinetics, pyrolysis gas flow through the porous char layer, and a mixture (solid and gas) energy equation. Verification results are presented for the thermochemical ablation of a carbon-phenolic ablator which invloves the solution of the entire system of governing equations.

Nomenclature

A	Area
$\mathbf{A}$	Area vector
a, b	Constants
B'_c	Dimensionless char ablation rate
C_h	Corrected heat transfer Stanton number
C_{h_o}	Uncorrected heat transfer Stanton number
C_m	Mass transfer Stanton number
C_p	Specific heat at constant pressure
C_v	Specific heat at constant volume
DE	Discretization error
$\dot{E}$	Element energy convection rate
$\tilde{E}$	Energy content

*This author is currently employed by NASA Johnson Space Center in Houston, TX, but the work was done while he was a graduate student at North Carolina State University and an intern at Sandia National Laboratories. AIAA Student Member.

†Sandia is a multiprogram laboratory operated by Sandia Corporation, a Lockheed Martin Company, for the United States Department of Energy's National Nuclear Security Administration under Contract DE-AC04-94AL85000.

‡Sandia National Laboratories consultant, Associate Fellow AIAA.

§Associate Professor, Department of Mechanical and Aerospace Engineering, Associate Fellow AIAA.

e	Specific internal energy
(e)	Element
h	Specific enthalpy
k	Thermal conductivity
L	Time dependent domain length
$\dot{m}''$	Mass loss rate per unit area
N	Shape function
Pr	Prandtl number
Q^*	Heat of ablation
$\dot{Q}$	Element heat conduction rate
$\dot{q}''$	Heat flux
$\dot{\mathbf{q}}''$	Heat flux vector
R	Residual
r	Recovery factor
s	Surface recession
$\dot{s}$	Surface recession rate
T	Temperature
t	Time
u	Control volume boundary velocity
$\mathbf{u}$	Velocity vector
V	Volume
x	Coordinate with respect to instantaneous ablation front
z	Coordinate with respect to initial ablation front
$\dot{z}$	Nodal velocity
α	Thermal diffusivity
δ	Perturbation
ϵ	Emissivity
η	Landau coordinate
θ	Transformed temperature
λ	Blowing reduction parameter
ξ	Local coordinate
ρ	Density
σ	Stefan-Boltzman constant
Ω	Stanton number correction

Subscript

abl	Ablation
ah	Aerodynamic heating
$back$	Back boundary
blw	Blowing
c	Char
cw	Cold wall
e	Boundary layer edge condition
$full$	Full sensitivity matrix
hw	Hot wall
$iter$	Iterative solution procedure
j	Nodal index
lag	Property lagging solution procedure
o	Initial value
r	Recovery value
rad	Radiation
ref	Reference value
res	Reservoir property
$surf$	Surface
tri	Tridiagonal sensitivity matrix
w	Property of gases adjacent to the wall

Superscript

n	Time level
ν	Iteration level
$*$	Reference value

I. Introduction

For nearly half of a century, numerical heat transfer and ablation modeling have been important tools in the design and analysis of rocket nozzles and re-entry vehicle heat-shields since they provide a means of simulating material thermal response including transient heat conduction, shape change, and in-depth decomposition. Accurate prediction of mass loss and energy transfer helps minimize vehicle weight while still maintaining the nozzle lining's or heat-shield's protective capabilities. In the 1960s, Moyer and Rindal[1] developed a one-dimensional, finite difference ablation code (Charring Materials Ablation, CMA) that employed a translating grid scheme in which the grid was attached to the receding surface and the overall number of nodes in the domain would be reduced as mass was removed at the ablating surface. With this method, each node translates with the same velocity as the surface and the size of grid cells remains fixed except for the back boundary cell which reduces in size until the cell has reached a critical thickness. This "node-dropping" translating grid scheme was a common approach during the 1960s and 1970s and is still used today.

Moyer and Rindal used a fully implicit time integrator and lagged the temperature dependent material properties and surface recession rate at the interior nodes while the nonlinear surface energy balance was solved iteratively to give the updated surface recession rate. Explicit integration of the solid energy equation has also been attempted by Moyer and Rindal during the development of CMA and more recently in a finite volume code by Suzuki et al.[2] In 1988, Blackwell[3] presented the control volume finite element method (CVFEM) for solving ablation problems on translating/node-dropping grids with a fully implicit time integrator with which he implemented the Moyer and Rindal approach to iterating only on the nonlinear surface energy balance.

Later, a contracting grid scheme for one-dimensional ablation was presented by Blackwell and Hogan[4] in which the relative size of grid cells and the total number of cells remains fixed throughout the problem, and each node translates at a fraction of the surface recession rate. This eliminates the node-dropping complexity, but adds a change in energy storage due to cell volume reduction. This method also has a more logical extension to multidimensional space as presented by Hogan et al.[5] Blackwell's and Hogan's work also implemented the CVFEM with a fully implicit time integrator that again iterated only on the surface energy balance to determine recession rate. More recent studies on one-dimensional and multidimensional ablation modeling and application work can be attributed to Suzuki et al.[6] and Chen and Milos.[7,8,9]

The current study is a presentation of the development and verification of a one-dimensional thermal response and ablation code using the CVFEM, a contracting grid scheme, and fully implicit time integration. Although the model has been developed for planar, cylindrical, and spherical geometries, only the solution for planar geometries is presented. This is a simplification to show the development, verification, and usability of the method. The governing equations are solved using the block Gauss-Seidel segregated solution procedure. Newton's method is used to iterate on the entire system of nodal residual equations to determine the time accurate temperature and density dependent properties and surface recession rate. Newton's method is only used to solve the segregated mixture energy and gas phase continuity equations while direct integration of the decomposition kinetics is used to update the solid density.

II. Governing Equations

The equations that govern the solid/gas system of the porous charring ablator include solid energy and continuity equations as well as the Navier-Stokes equations as applied to all of the gaseous species considered. In the general case, it is possible that the pyrolysis gases react among themselves, erode the remaining solid, or deposit residue (coke) on the solid, but these phenomena are neglected. Under the assumptions that the pyrolysis gas is a single nonreactive entity, the solid and gas are in thermal equilibrium, and there is no in-depth energy source, then the solid and gas energy equations for a moving grid reduce to a mixture

energy equation given by

$$\underbrace{\int_{cs} \dot{\mathbf{q}}'' \cdot d\mathbf{A}}_{\text{conduction}} + \underbrace{\int_{cs} \phi \rho_g h_g \mathbf{v}_g \cdot d\mathbf{A}}_{\text{gas flux}} - \underbrace{\int_{cs} \rho h \mathbf{v}_{cs} \cdot d\mathbf{A}}_{\text{grid convection}} + \frac{d}{dt} \underbrace{\int_{cv} \rho e dV}_{\text{energy content}} = 0 \tag{1}$$

and the mixture continuity equation is

$$\underbrace{\int_{cs} \phi \rho_g \mathbf{v}_g \cdot d\mathbf{A}}_{\text{gas flux}} - \underbrace{\int_{cs} \rho \mathbf{v}_{cs} \cdot d\mathbf{A}}_{\text{grid convection}} + \frac{d}{dt} \underbrace{\int_{cv} \rho dV}_{\text{mass content}} = 0 \tag{2}$$

which is the sum of the solid and gas phase continuity equations given by

$$\text{solid: } \frac{d}{dt} \underbrace{\int_{cv} \rho_s dV}_{\text{solid mass content}} - \underbrace{\int_{cs} \rho_s \mathbf{v}_{cs} \cdot d\mathbf{A}}_{\text{grid convection}} = \underbrace{\int_{cv} \dot{m}_s''' dV}_{\text{solid mass source}} \tag{3}$$

and

$$\text{gas: } \frac{d}{dt} \underbrace{\int_{cv} \phi \rho_g dV}_{\text{gas mass content}} + \underbrace{\int_{cs} \phi \rho_g \mathbf{v}_g \cdot d\mathbf{A}}_{\text{gas flux}} - \underbrace{\int_{cs} \phi \rho_g \mathbf{v}_{cs} \cdot d\mathbf{A}}_{\text{grid convection}} = \underbrace{\int_{cv} \dot{m}_g''' dV}_{\text{gas mass source}} \tag{4}$$

where

$$\int_{cv} \dot{m}_g''' dV + \int_{cv} \dot{m}_s''' dV = 0 \tag{5}$$

Applying the Navier-Stokes momentum equations to flow through the char layer would require detailed knowledge of the pore structure, and that information is not known. Instead we use Darcy's law which relates the volumetric flow rate ($\boldsymbol{Q}$) of a laminar flowing fluid to the local pressure gradient within a fully saturated porous medium by

$$\boldsymbol{Q} = -A \frac{\kappa}{\mu} \nabla P \tag{6}$$

The superficial or filtration velocity is the volumetric flow rate averaged over the cross-sectional area of the medium and is given by

$$\mathbf{v}' = \frac{\boldsymbol{Q}}{A} = -\frac{\kappa}{\mu} \nabla P \tag{7}$$

Since the momentum equation for the pyrolysis gases is assumed to be Darcy's law, which provides a simple relationship between fluid velocity and the pressure gradient, Darcy's law in conjunction with the perfect gas law is treated as a closure relationship for the energy-continuity system of equations with surface recession rate, temperature, solid density, and gas density being the dependent variables. As a result, there is no independent solution of a momentum equation since this is inherent in the gas phase continuity equation solution.

The block Gauss-Seidel procedure uses Newton's method for a system of nonlinear equations to solve the segregated mixture energy and gas phase continuity equations. Consequently, a residual formulation, or Δ-formulation, of the control volume energy and gas mass balance equations is solved resulting in the linear system's Jacobian matrix, $[A]$ in Eq. 8, being comprised of the residuals' sensitivities to the dependent variables.

$$[A]\, \boldsymbol{\Delta x} = \mathbf{R} \tag{8}$$

As a result, convergence can be monitored as the correction vector, $\boldsymbol{\Delta x}$, or the residual vector, $\mathbf{R}$, approaches zero. The solid continuity equation is not solved in this manner and is instead solved through direct integration of the decomposition kinetics.

The solution procedure for the entire system of governing equations can be outlined as follows:

1. Iteratively solve the mixture energy equation with nodal temperatures and surface recession rate as the dependent variables

- Adjust grid throughout iteration procedure (the contracting grid scheme is described in the previous paper[10] and Amar[11])
- Hold nodal density and gas velocity values constant

2. Integrate kinetic relationships to solve solid phase continuity equation
   - Use updated grid and temperature field
3. Iteratively solve the gas phase continuity equation with nodal gas densities as the dependent variables
   - Use Darcy's law to determine pyrolysis gas velocity in the pore space
   - Hold solid density, temperature, and recession rate constant from previous converged solution of the energy and solid continuity equations

This segregated solution procedure in which updated information is being used as soon as it is available is commonly referred to as the block Gauss-Seidel method which converges linearly if implemented correctly. Steps 1-3 are repeated until global convergence of the Gauss-Seidel method is reached, and the system is considered globally converged when no local nonlinear iteration is necessary to converge the mixture energy equation.

III. Mixture Energy Equation

derivation details will be in full paper

IV. Solid Phase Continuity Equation

Since the solid density gradient in the decomposition region is known to be much larger than the temperature gradients in the domain, a finer mesh is necessary for the solution of the solid phase continuity equation than was needed to solve the energy equation. CMA and several other studies employ a sub-mesh scheme in which there are a given number of nodelets (or sub-nodes) within each element on which the solid phase continuity equation is solved. Integral effects of the nodelet solutions are applied at nodes during the solution of the mixture energy equation. This method saves a significant amount of computational time since it avoids excessive grid points during the mixture energy equation solution. The nodelet scheme has not been implemented in the current model, therefore each governing equation is solved on the same mesh.

Implicit integration of the solid mass conservation equation through the CVFEM and nodal mass balance equations is not performed. Instead, direct integration of the kinetic relationships accounting for the moving grid, which has been used in previous studies,[1] was chosen to determine the solution. The development of the fixed grid solid continuity equation solution procedure is presented, and the moving grid effects are considered afterwards.

A. Solution Procedure

The solid phase continuity equation on a fixed grid is given by

$$\frac{d}{dt} \underbrace{\int_{cv} \rho_s dV}_{\text{solid mass content}} = \underbrace{\int_{cv} \dot{m}_s''' dV}_{\text{solid mass source}} \tag{9}$$

where

$$\rho_s = \underbrace{\Gamma\left(\rho_A + \rho_B\right)}_{\text{resin}} + \underbrace{\left(1-\Gamma\right)\rho_C}_{\text{binder}} \tag{10}$$

Substituting Eq. 10 into Eq. 9 and knowing that the component source terms can be volumetrically weighted like the component densities gives

$$\frac{d}{dt}\int_{cv} \left[\Gamma\left(\rho_A + \rho_B\right) + \left(1-\Gamma\right)\rho_C\right] dV = \int_{cv} \left[\Gamma\left(\dot{m}_A''' + \dot{m}_B'''\right) + \left(1-\Gamma\right)\dot{m}_C'''\right] dV \tag{11}$$

Since the decomposition of each component is independent of the other components when coupling effects from the other governing equations are ignored, the solid phase continuity equation can be further reduced to component continuity equations given by

$$\frac{d}{dt}\int_{cv}\rho_i dV = \int_{cv}\dot{m}_i'''dV \text{ for } i = A,\ B, \text{ and } C \tag{12}$$

Now there are four equations (Eqs. 11 and 12) with four unknowns (ρ_A, ρ_B, ρ_C, and ρ_s), and the procedure is to solve the component continuity equations and then determine the solid density as a post-processing step via Eq. 10. The analogous finite difference relationship to Eq. 12 is

$$\left.\frac{\partial\rho_i}{\partial t}\right|_z = \dot{m}_i''' = -k_i\rho_{v_i}\left(\frac{\rho_i-\rho_{c_i}}{\rho_{v_i}}\right)^{\psi_i}e^{-E_i/RT} \text{ for } i = A,\ B, \text{ and } C \tag{13}$$

Since the density history at a given location only depends on the temperature history at that location, Eq. 13 can be integrated on a location-by-location basis (accounting for the moving grid) and the updated solid density can be determined.

B. Integration of Kinetic Equations

Since ρ_{v_i} and ρ_{c_i} are constants, the kinetic equation in Eq. 13 can be rearranged to give

$$\left.\frac{dw_i}{dt}\right|_z = -k_i w_i^{\psi_i}e^{-E_i/RT} \text{ for } i = A,\ B, \text{ and } C \tag{14}$$

where the dimensionless relative density is given by

$$w_i = \frac{\rho_i-\rho_{c_i}}{\rho_{v_i}} \tag{15}$$

Direct integration of Eq. 14 over one time step while treating temperature explicitly in time, gives

$$w_i\left(z_j^{n+1},t^{n+1}\right) = \left\{\left[w_i\left(z_j^{n+1},t^n\right)\right]^{(1-\psi_i)} - \Delta t^{n+1}\left(1-\psi_i\right)k_i e^{-E_i/RT\left(z_j^{n+1},t^n\right)}\right\}^{\frac{1}{1-\psi_i}} \tag{16}$$

$$\text{for } \psi_i \neq 1$$

and

$$w_i\left(z_j^{n+1},t^{n+1}\right) = \left[w_i\left(z_j^{n+1},t^n\right)\right]e^{-k_i\Delta t^{n+1}e^{-E_i/RT\left(z_j^{n+1},t^n\right)}} \tag{17}$$

$$\text{for } \psi_i = 1$$

Eqs. 16 and 17 were implemented in CMA to integrate the kinetic equations regardless of the temperature change over the time interval. They are applied in the current model only if the temperature remains constant over the time interval $\left[T\left(z_j^{n+1},t^{n+1}\right) = T\left(z_j^{n+1},t^n\right)\right]$.

An alternative approach to determining the dimensionless relative densities at time level $n+1$ is to assume that the temperature rise rate over the time interval Δt^{n+1} is a constant, Θ.

$$\left.\frac{dT}{dt}\right|_z = \Theta = \frac{T\left(z_j^{n+1},t^{n+1}\right) - T\left(z_j^{n+1},t^n\right)}{\Delta t} \tag{18}$$

This is consistent with the implicit time integrator's ability to at best capture a linear temperature rise rate since the method is first order. Using Eq. 14 and the chain rule gives

$$\left.\frac{dw_i}{dT}\right|_z \Theta = -k_i w_i^{\psi_i}e^{-E_i/RT} \text{ for } i = A,\ B, \text{ and } C \tag{19}$$

Integrating and solving for $w_i\left(z_j^{n+1}, t^{n+1}\right)$ gives

$$w_i\left(z_j^{n+1}, t^{n+1}\right) = \left\{ \left[w_i\left(z_j^{n+1}, t^n\right)\right]^{1-\psi_i} + \frac{k_i\left(\psi_i - 1\right)}{\Theta} \int_{T\left(z_j^{n+1}, t^n\right)}^{T\left(z_j^{n+1}, t^{n+1}\right)} e^{-E_i/RT} dT \right\}^{\frac{-1}{\psi_i - 1}} \tag{20}$$

$$\text{for } \psi_i \neq 1$$

and

$$w_i\left(z_j^{n+1}, t^{n+1}\right) = \exp\left(\ln\left[w_i\left(z_j^{n+1}, t^n\right)\right] - \frac{k_i}{\Theta} \int_{T\left(z_j^{n+1}, t^n\right)}^{T\left(z_j^{n+1}, t^{n+1}\right)} e^{-E_i/RT} dT \right) \tag{21}$$

$$\text{for } \psi_i = 1$$

$\int_{T\left(z_j^{n+1}, t^n\right)}^{T\left(z_j^{n+1}, t^{n+1}\right)} e^{-E_i/RT} dT$ can be determined through the use of exponential integrals or numerical integration techniques, and Simpson's rule was chosen for this study. Since the new dimensionless relative densities are known, the component densities can be determined via Eq. 15, and the solid bulk density can now be determined from

$$\rho_s^{n+1} = \Gamma\left(\rho_A^{n+1} + \rho_B^{n+1}\right) + \left(1 - \Gamma\right)\rho_C^{n+1} \tag{22}$$

or in terms of dimensionless relative densities

$$\rho_s^{n+1} = \rho_{c_s} + \Gamma\left(\rho_{v_A} w_A^{n+1} + \rho_{v_B} w_B^{n+1}\right) + \left(1 - \Gamma\right)\rho_{v_C} w_C^{n+1} \tag{23}$$

Since problems are solved on contracting grids for which the spatial coordinate of each node changes while the Landau coordinate of each node is fixed, it is necessary to determine temperature and dimensionless relative density profiles at the previous time level and current nodal locations $\left(T\left(z_j^{n+1}, t^n\right)\right.$ and $\left.w_i\left(z_j^{n+1}, t^n\right)\right)$. Since properties are assumed to vary linearly within elements, linear interpolation in the old (time level n) profiles is used to calculate these properties.

V. Gas Phase Continuity Equation

derivation details will be in full paper

VI. Verification Results: Thermochemical Ablation of a Decomposing Material

A. Problem Statement

Since most of the energy equation terms and boundary conditions have been previously verified (see the previous paper[10] and Amar[11]), the decomposing material thermochemical ablation problem is intended to verify the implementation of the gas phase continuity equation in addition to the pyrolysis gas effects in the mixture energy equation. Due to the difficulty in determining an analytical solution, Richardson extrapolation is used to approximate the exact solution, and the global convergence rate and nonlinear convergence rates of the mixture energy and gas phase continuity equations are determined.

Consider a 0.5 inch thick planar slab of carbon-phenolic (with material properties given in Amar[11]) that is subject to a typical heating load characteristic of a ballistic sphere-cone re-entry body. The Stanton number is corrected for both hot wall and blowing effects and the surface is subject to a far-field radiation condition where the source temperature is 414.0 °R. The back boundary is adiabatic and impermeable, and the time dependent specified surface pressure is provided by the aerodynamic heating boundary condition input.

B. Grid Refinement Studies

The domain was discretized with a series of four grids with $\Delta t/\Delta z_o^2 =$ constant, and the grid parameters can be seen in Table 1. Since the solid continuity equation is solved through direct integration of the

Table 1. Parameters for carbon-phenolic thermochemical ablation problem grid refinement study.

Grid	# elem	Δz_o, in	Δt, s
coarse	50	0.01	0.1
medium	100	0.005	0.025
fine	200	0.0025	0.00625
extra-fine	400	0.00125	0.0015625

decomposition kinetics, it is unclear how its solution and consequently its coupling with the other governing equations will behave as the mesh is refined. As a result, an alternative procedure to the previous verification problems was used in order to isolate the mixture energy and gas phase continuity equations from the solid phase continuity equation solution. The procedure is as follows:

1. Solve the problem on the extra-fine mesh until a problem time of $t = 25\,\mathrm{s}$ is reached
2. The conditions found at $t = 25\,\mathrm{s}$ can then be used to re-initialize the problem on the entire series of grids resulting in
   - Nonuniform initial profiles for:
     a. Temperature
     b. Solid density
     c. Porosity
     d. Permeability
     e. Gas density
     f. Gas generation rate
     g. Gas velocity
   - Contracted grid
   - Re-initialization during an ablating interval
3. Verify the mixture energy equation
   - Integrate over 0.1 s (restarting at $t = 25\,\mathrm{s}$) for the entire series of grids only advancing the mixture energy equation in time while holding all other terms constant
     a. Integration over a small time interval reduces errors associated with inconsistent nodal locations
     b. Result is as revealing as integrating over a long time interval if all of the relevant terms are being employed which is ensured by the nonuniform initialization
   - Perform Richardson extrapolation at $t = 25.1\,\mathrm{s}$ on the surface temperature, recession rate, and back face temperature. The results showing the second order grid convergence can be seen in Figure 1.

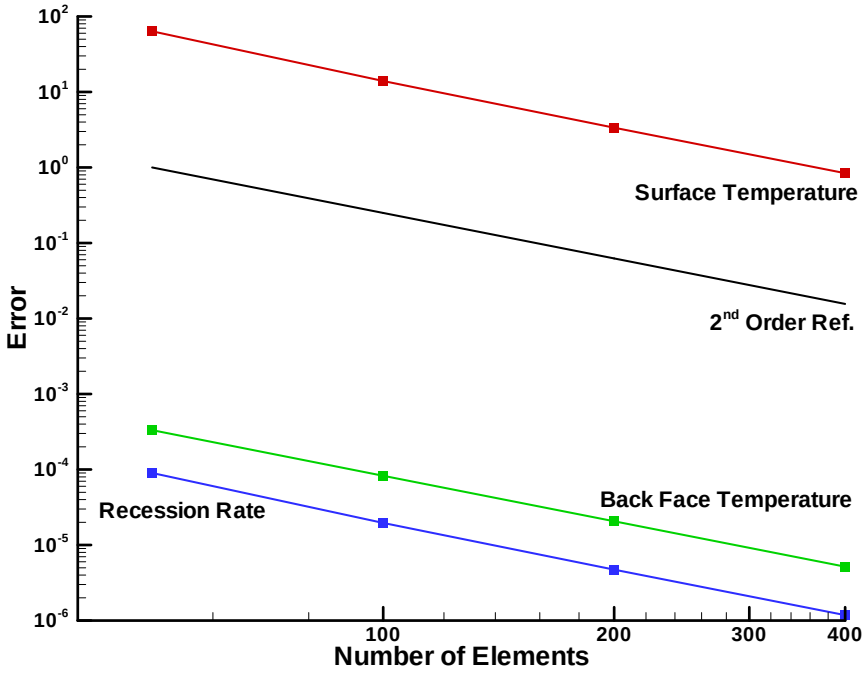

Figure 1. Mixture energy equation grid convergence results for carbon-phenolic thermochemical ablation verification problem.

4. Verify the gas phase continuity equation

   - Integrate over 1.0 s (restarting at $t = 25\,\mathrm{s}$) for the entire series of grids only advancing the gas phase continuity equation in time while holding all other terms constant
   - Perform Richardson extrapolation at $t = 26.0\,\mathrm{s}$ on the surface gas flux, an interior gas density value at a consistent spatial location, and back face gas density. The results showing the second order grid convergence can be seen in Figure 2.

     a. An interior location is chosen for Richardson extrapolation on the gas density because the surface gas density is specified through the boundary conditions. $z = 1.07 \times 10^{-2}\,\mathrm{in}$ is the position of the first interior node on the coarsest mesh which has a collocated node on each of the finer meshes.

     b. Integration over a longer time interval was performed since the mesh does not contract during the solution of the gas phase continuity equation

C. Nonlinear Convergence Studies

For the mixture energy equation, the error metric used to determine the nonlinear convergence rate is the recession rate as given by

$$(error)^{\nu} = (\dot{s})^{\nu} - (\dot{s})^{converged} \tag{24}$$

and the error metric for the gas phase continuity equation is the relative L_2 norm of the density correction vector.

$$(error)^{\nu} = (L_2)^{\nu} - (L_2)^{converged} \tag{25}$$

The convergence rates are shown in Figures 3 and 4, and the results follow the second order line.

The block Gauss-Seidel method used to solve the entire system of governing equations is expected to exhibit linear convergence. Since the solution procedure achieves coupling through iteration, information can only be used as soon as it is updated and a smooth convergence curve should not be expected. To examine the global convergence, it is necessary to view the problem in global iteration space as opposed to

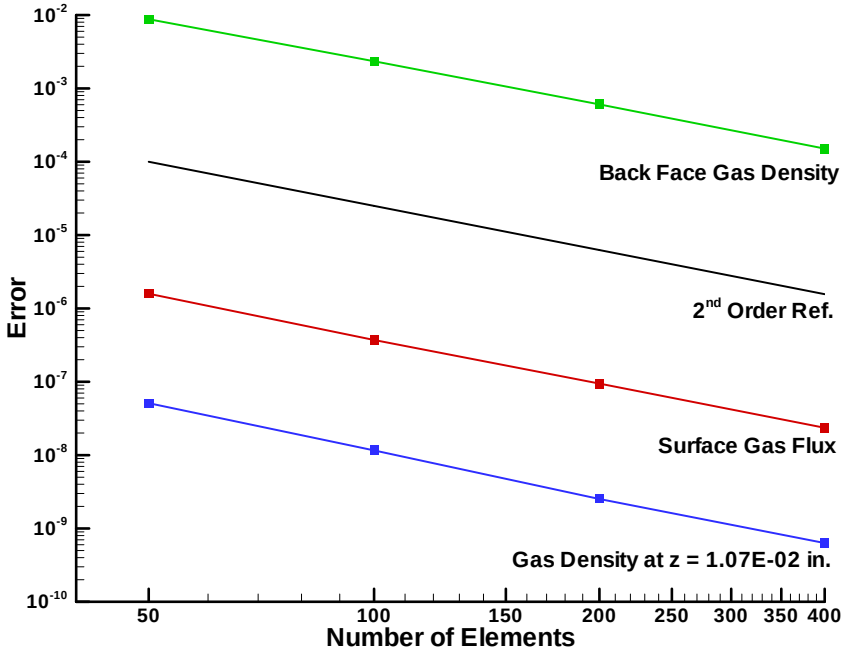

Figure 2. Gas continuity equation grid convergence results for carbon-phenolic thermochemical ablation verification problem.

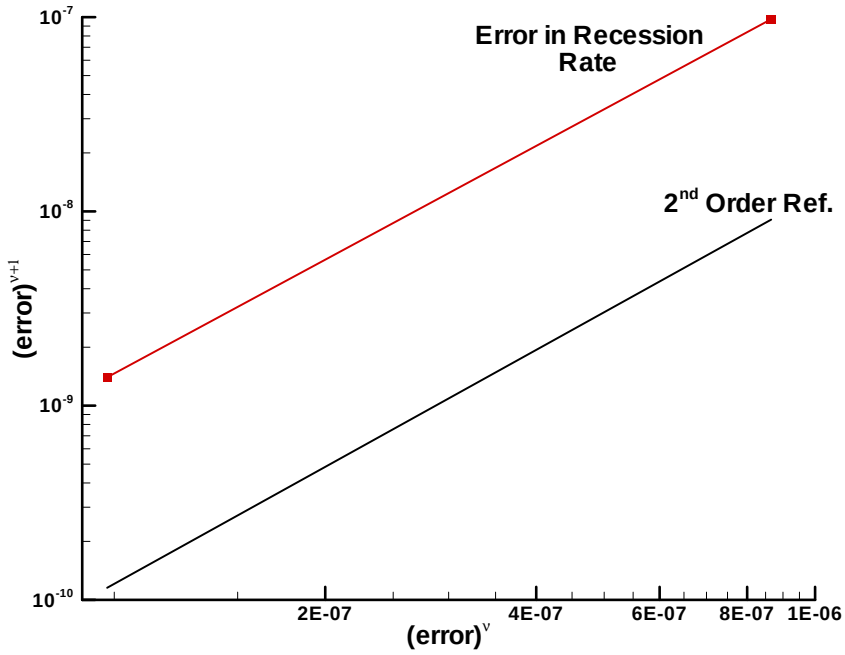

Figure 3. Nonlinear convergence of surface recession rate for carbon-phenolic thermochemical ablation verification problem.

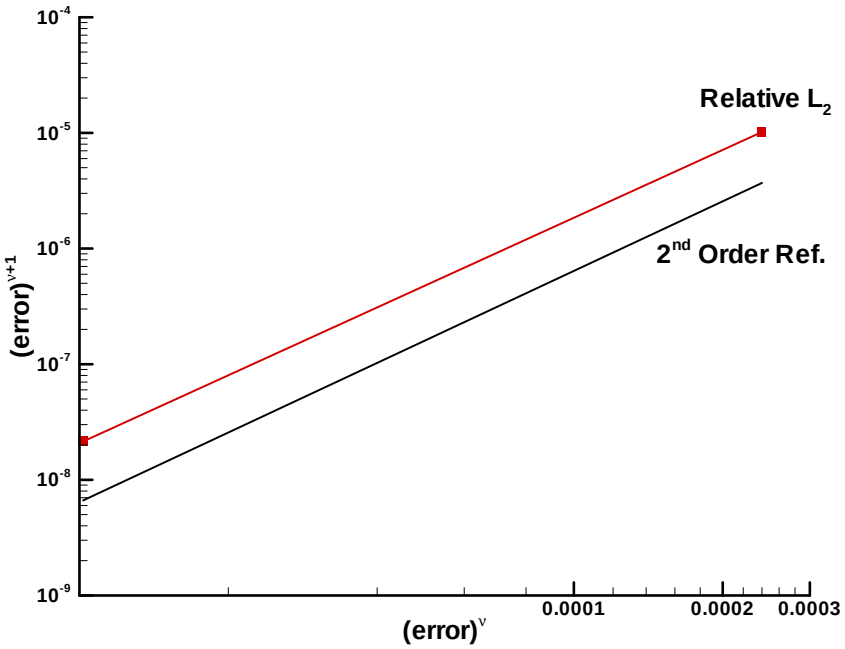

Figure 4. Nonlinear convergence of gas continuity equation's L_2 error norm for the carbon-phenolic thermochemical ablation verification problem.

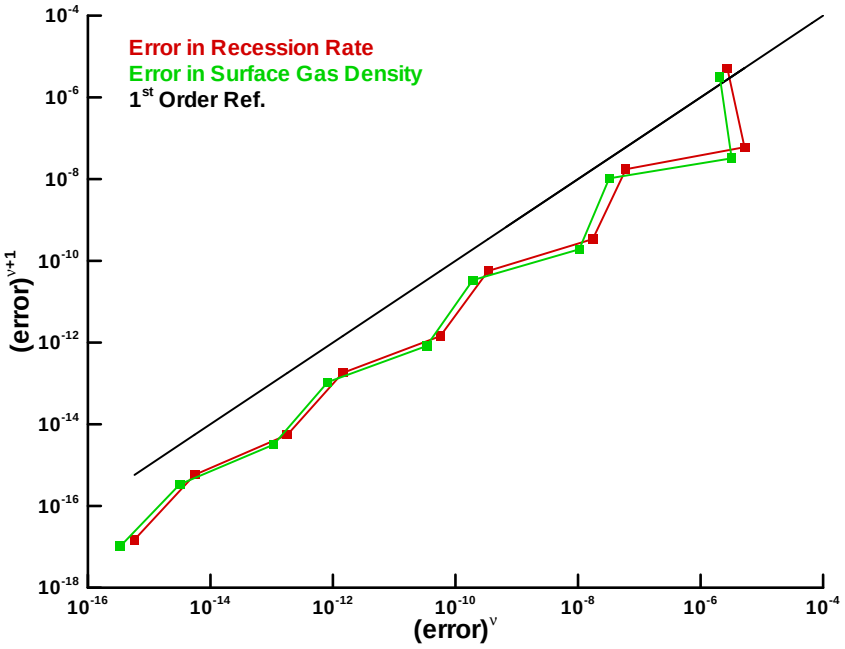

Figure 5. Global convergence rate for surface recession rate and gas density where ν is the global iteration index.

local (Newton) iteration space. Let the iteration index (ν) now represent the global iteration. Since the solution globally converges to the exact solution plus some discretization error, the difference between the locally converged solution at a given global iteration (X^{ν}) and the globally converged solution ($X^{g.c.}$) is used as the error metric.

$$(error)^{\nu} = X^{\nu} - X^{g.c.} \tag{26}$$

The global convergence rates of the surface recession rate and gas density are shown in Figure 5 while the global convergence rates for the surface temperature and solid density are shown in Figure 6. It is important to note that the surface gas density only changes with surface temperature since the boundary pressure is known from the boundary conditions. As a result, the surface gas density and temperature will always converge to machine precision in the same number of global iterations. On the other hand, the surface solid density reaches global convergence in fewer iterations and experience has shown that this is generally the case.

D. Code-to-Code Comparison

Although code-to-code comparisons are not part of the formal verification process, comparisons with established codes were performed to see how the improved scheme changes the final solution. The carbon-phenolic thermochemical ablation problem was solved on the medium grid in Table 1 using both CMA and the code developed during this study. Although CMA has the capability to integrate the decomposition kinetics on a finer mesh than is used to solve the mixture energy equation, this option was not exercised in order to make a more direct comparison. It is also important to note that the primary differences between the two codes for this simulation are as follows:

1. CMA iterates only on the surface energy balance and lags temperature dependent properties and surface recession rate for the interior node solution while the research code iterates on the entire system of residual equations to determine time accurate nonlinearities

2. CMA uses a translating/node-dropping grid scheme, and the research code uses a contracting grid scheme

3. CMA uses a lumped capacitance method, and the research code uses a distributed capacitance method

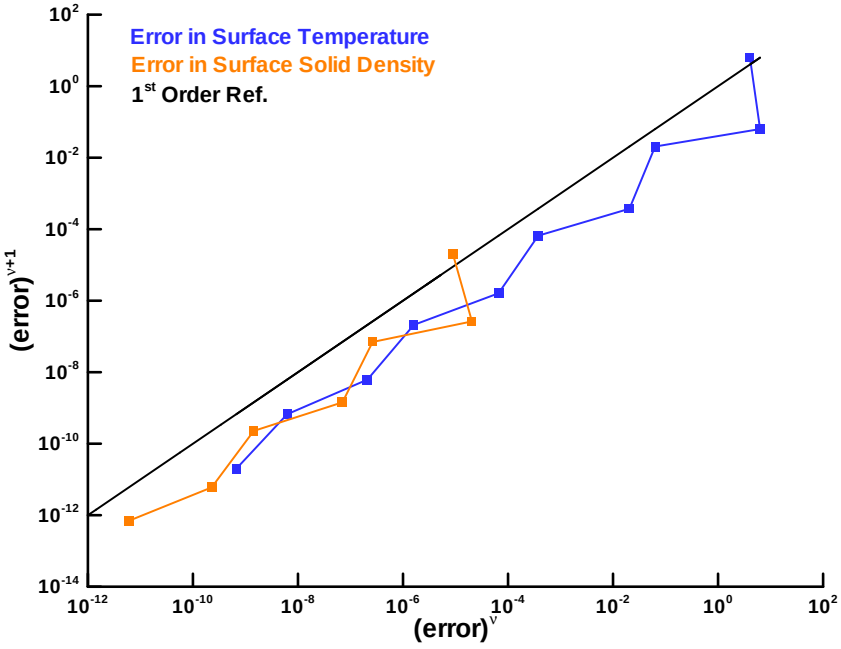

Figure 6. Global convergence rate for surface temperature and solid density where ν is the global iteration index.

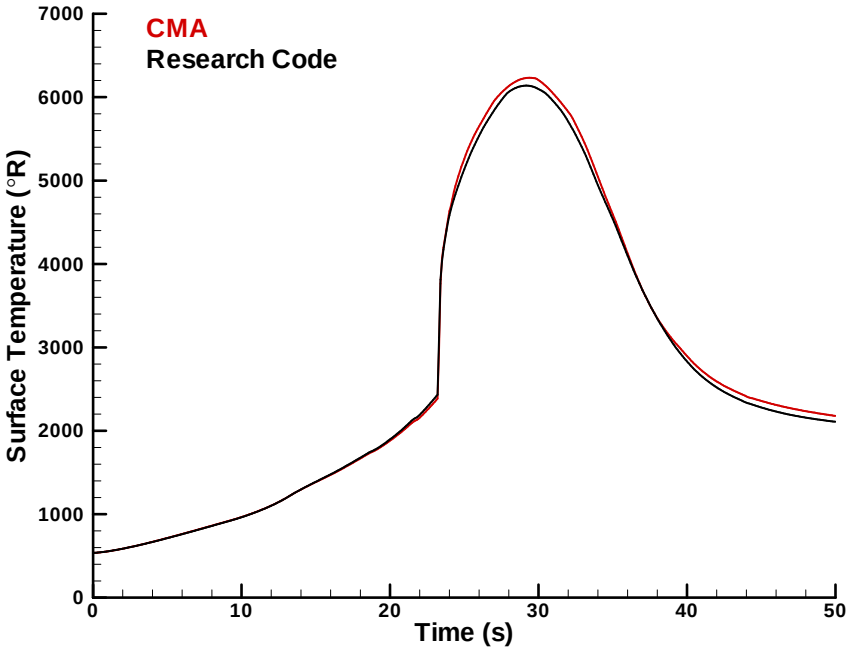

Figure 7. Comparison of surface temperature predictions for the carbon-phenolic thermochemical ablation verification problem.

4. CMA linearly interpolates on $\ln(B'_c)$, and the research code linearly interpolates on B'_c
5. CMA assumes that all gas generated further in-depth than a given node passes that node in the time interval in which the gas was generated and the flow work is accounted for, and the research code allows internal pressure gradients to drive the flow of pyrolysis gases through the pore space
6. CMA does not account for the gas phase internal energy in the energy capacitance term, and the research code does account for the gas phase internal energy

The comparisons for the predicted surface temperature, back face temperature, recession, and recession rate histories can be seen in Figures 7, 8, 9, and 10 respectively. Due to the number of numerical differences between the codes and the number of physical phenomenon that are being modeled throughout the solution procedure, it is difficult to discern what modeling differences between the two codes is causing the discrepancy in the solutions. From these results it is evident that CMA's pyrolysis gas assumptions, described in items 5 and 6 in the above list, are valid since including the porous flow solution (as is done in the research code) does not significantly change the mixture energy equation solution. This suggests a dominantly one-way coupling between the mixture energy equation and the gas phase continuity equation, which is expected since gas velocities are low and the heat capacity and thermal conductivity for gases are generally much lower than they are for a solid.

E. Porous Flow Results

One of the primary goals of this study is the implementation and verification of the gas phase continuity equation with porous flow assumptions in order to predict in-depth pressure in a charring ablator. Figures 11-19 show profile histories for several properties in the charring carbon-phenolic ablator including gas density, pressure, and gas superficial velocity, which are predicted through solving the gas phase continuity equation with porous flow assumptions. It is evident that the gas density, pressure, and solid decomposition (or gas generation) rate profiles have steep gradients when compared to the temperature profile. This suggests that if a sub-mesh scheme is implemented, then both the solid and gas phase continuity equations should be solved on the sub-mesh. In addition, the apparent "kinks" in the permeability profiles in Figure 19 are a result of the available permeability data that was used for the simulation.

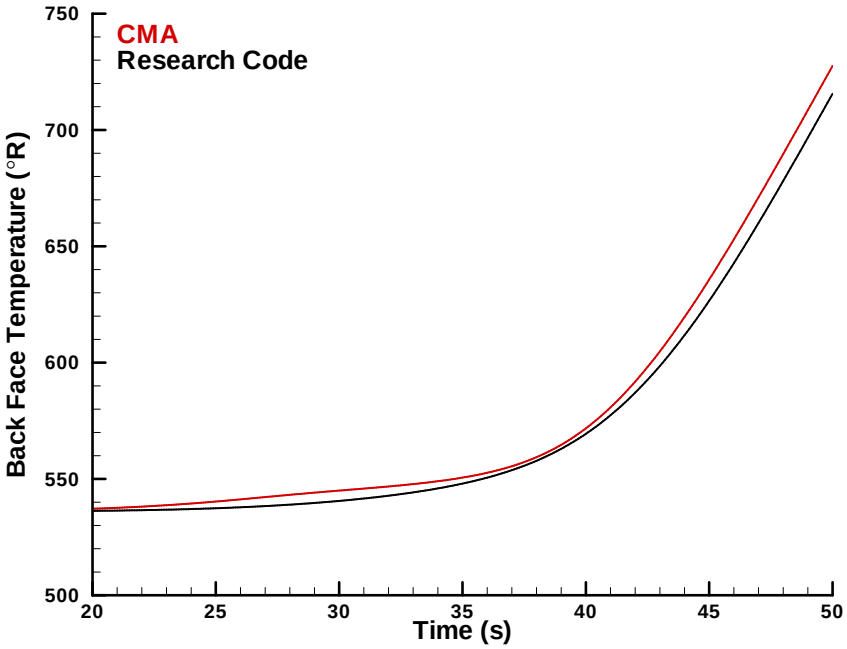

Figure 8. Comparison of back face temperature predictions for the carbon-phenolic thermochemical ablation verification problem.

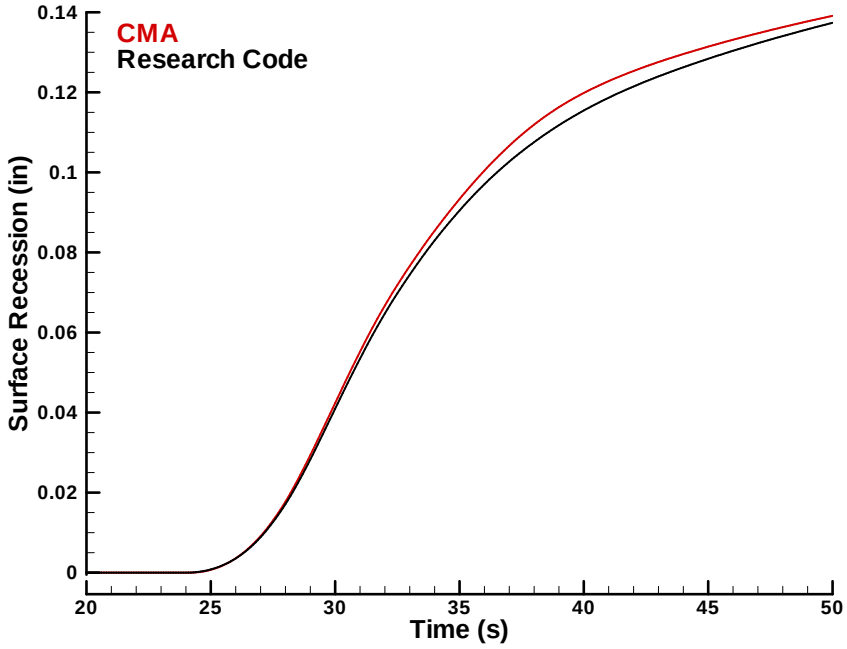

Figure 9. Comparison of surface recession predictions for the carbon-phenolic thermochemical ablation verification problem.

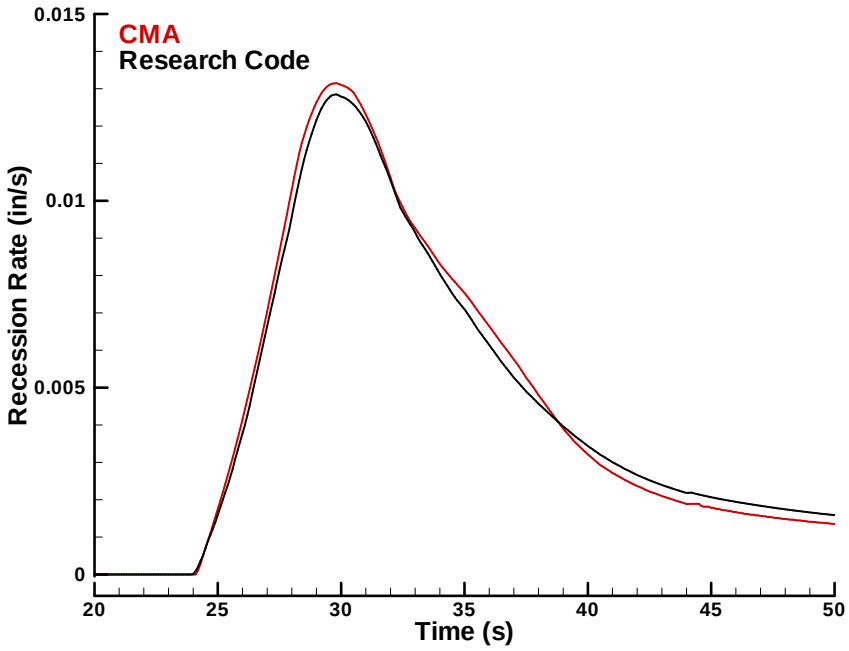

Figure 10. Comparison of surface recession rate predictions for the carbon-phenolic thermochemical ablation verification problem.

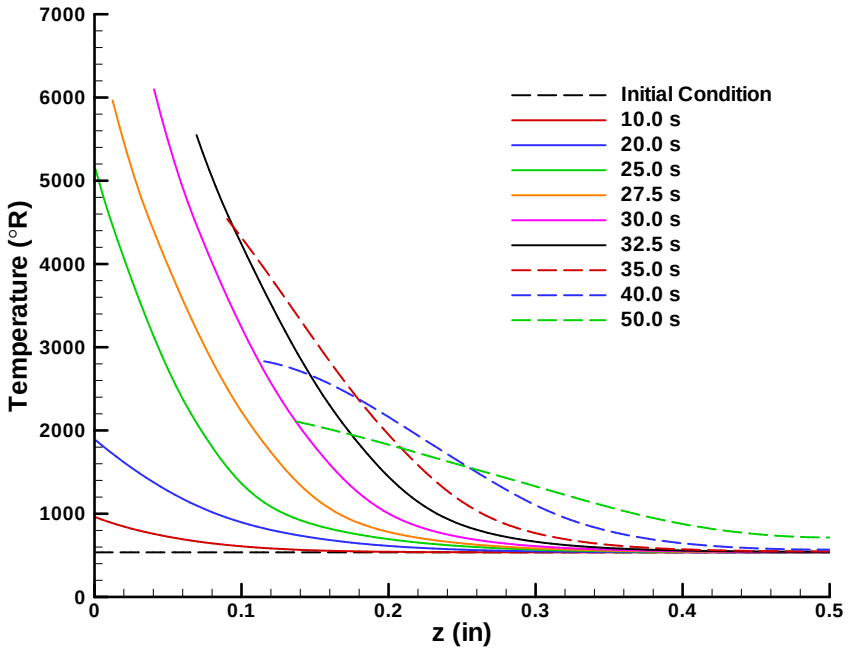

Figure 11. Temperature profile history for the carbon-phenolic thermochemical ablation verification problem.

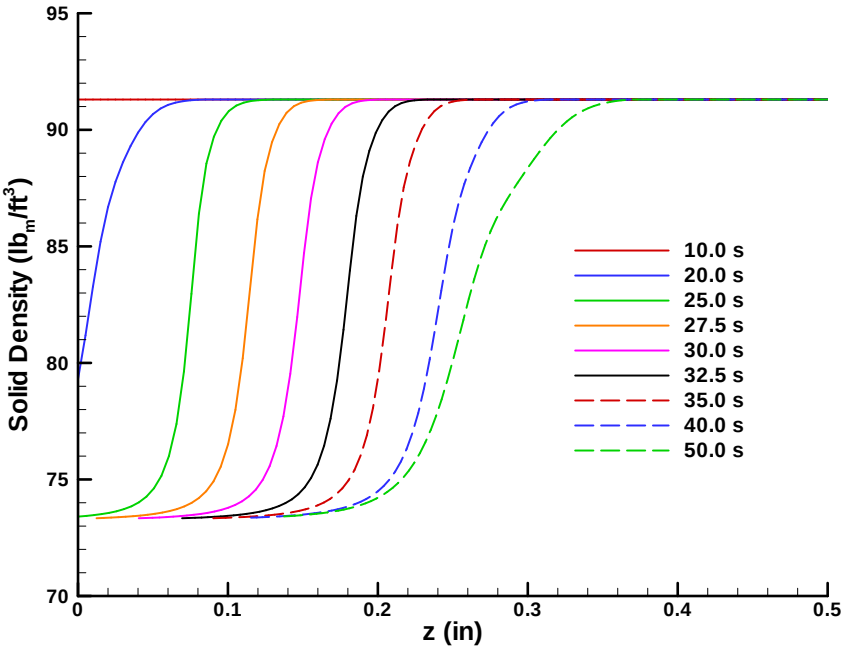

Figure 12. Solid density profile history for the carbon-phenolic thermochemical ablation verification problem.

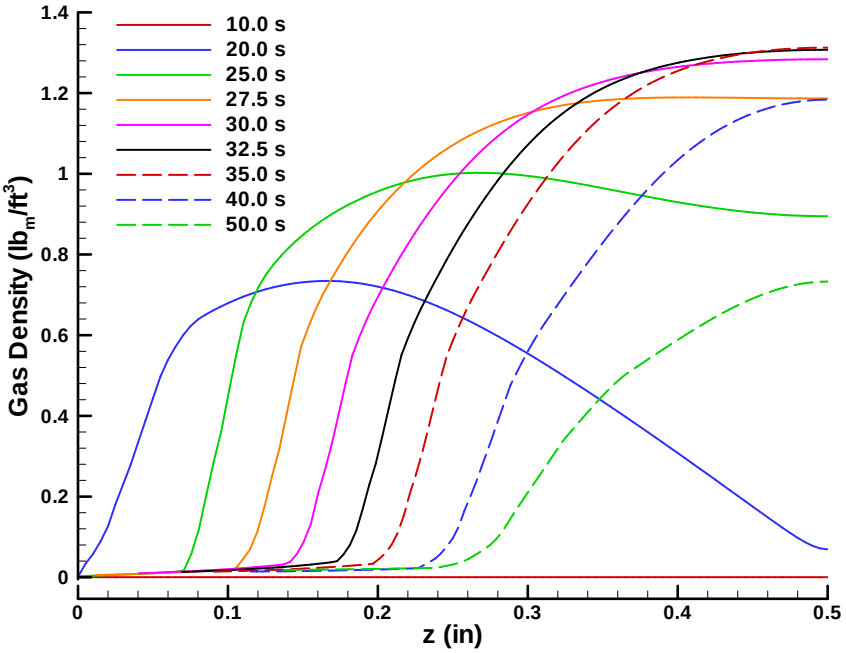

Figure 13. Gas density profile history for the carbon-phenolic thermochemical ablation verification problem.

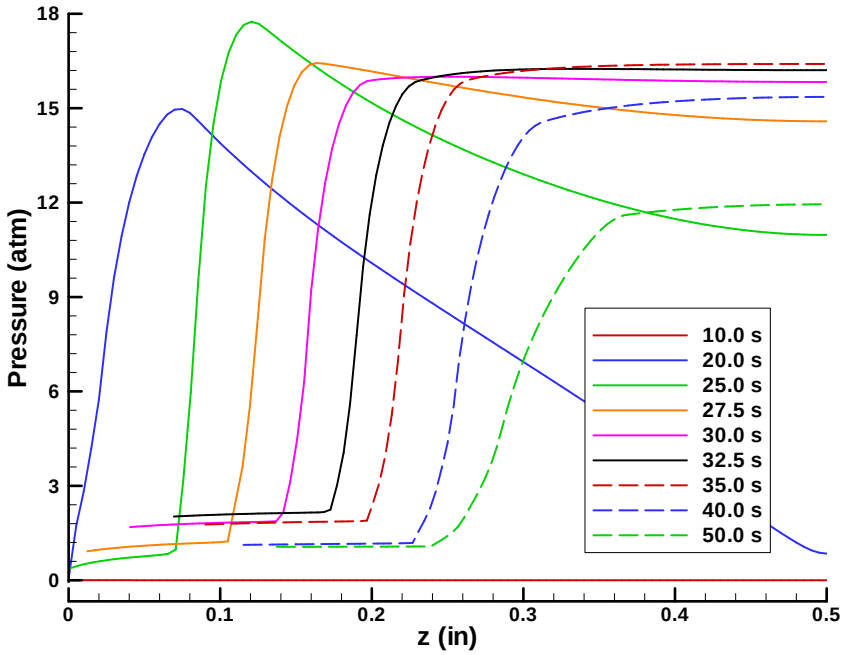

Figure 14. Pressure profile history for the carbon-phenolic thermochemical ablation verification problem.

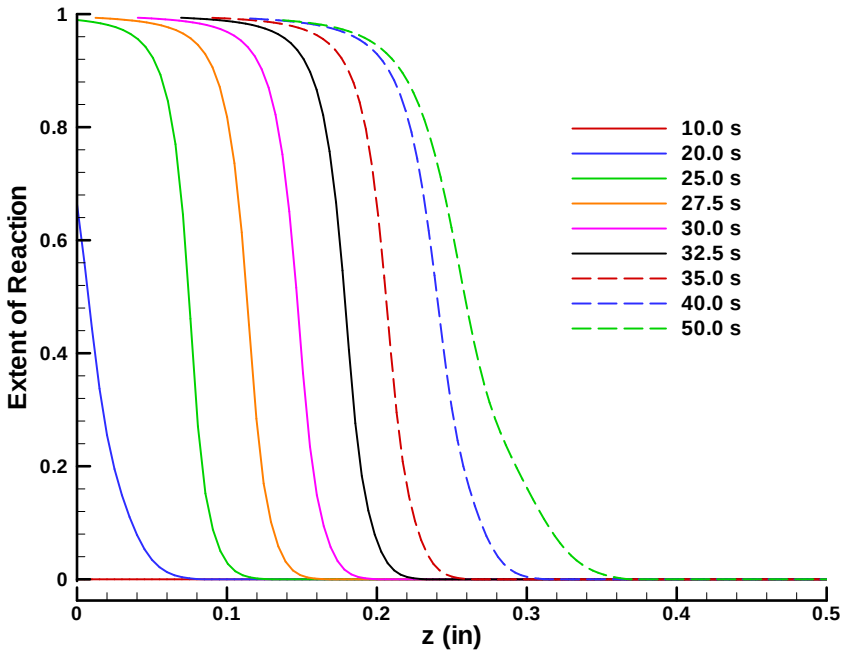

Figure 15. Extent of reaction (β) profile history for the carbon-phenolic thermochemical ablation verification problem.

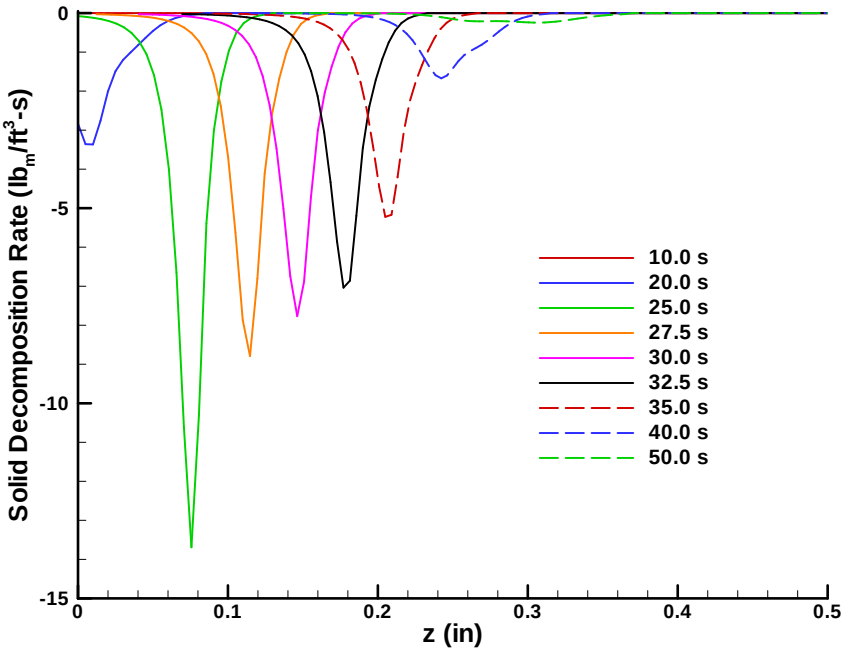

Figure 16. Solid decomposition rate profile history for the carbon-phenolic thermochemical ablation verification problem.

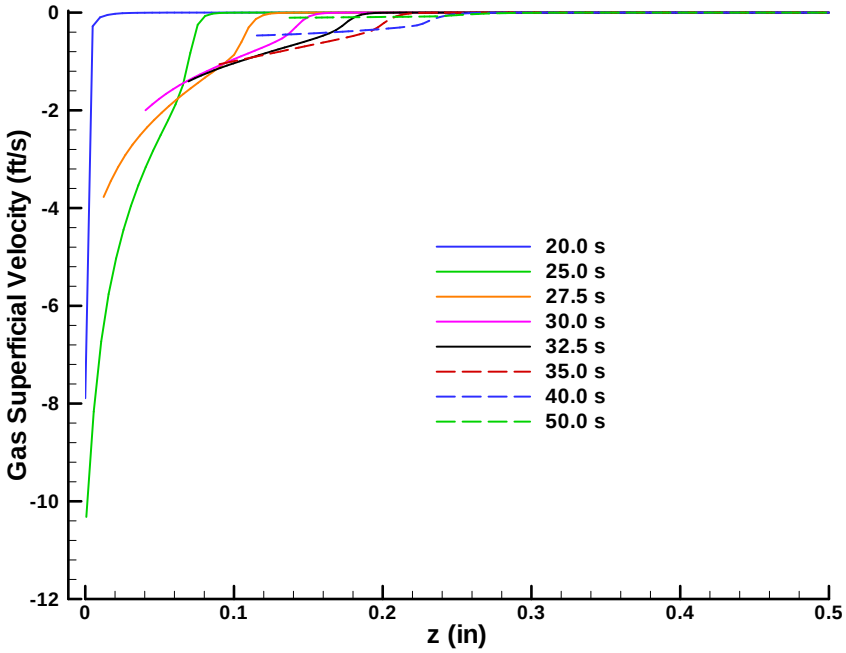

Figure 17. Gas superficial velocity profile history for the carbon-phenolic thermochemical ablation problem where a negative velocity is toward the ablating surface.

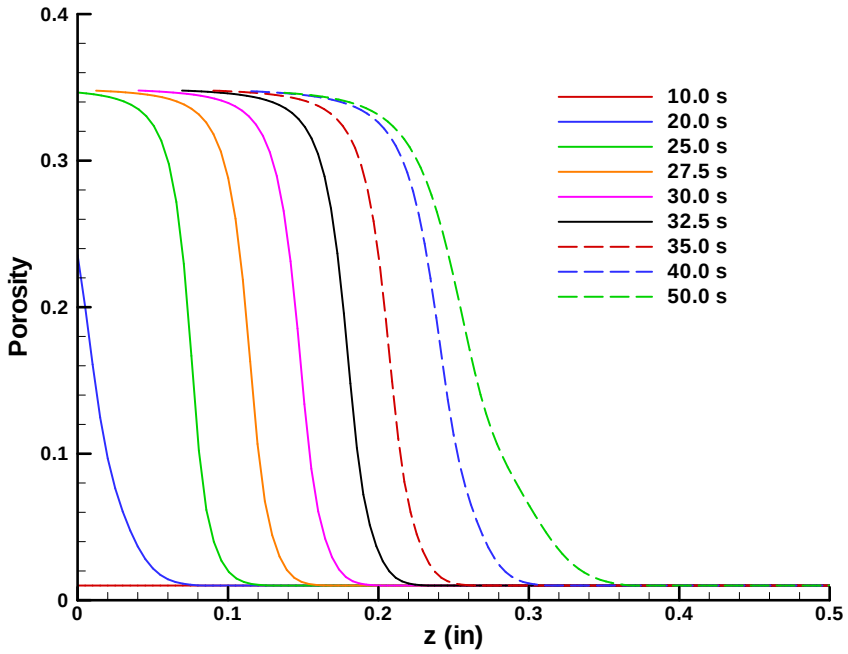

Figure 18. Porosity profile history for the carbon-phenolic thermochemical ablation verification problem.

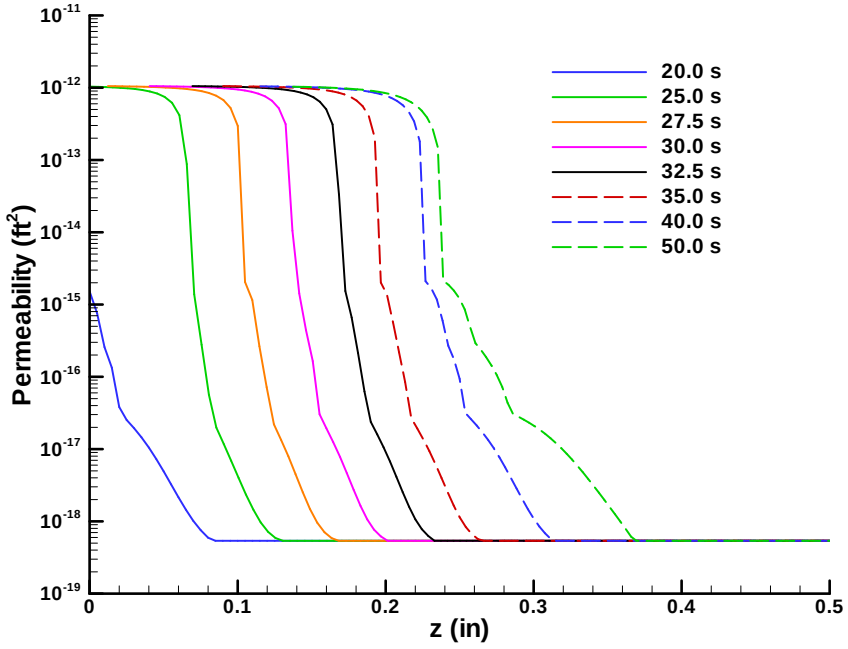

Figure 19. Permeability profile history for the carbon-phenolic thermochemical ablation verification problem.

Figure 15 shows that ablation begins to occur before the surface solid becomes fully charred meaning that there is still non-decomposed resin in the solid. This creates a discrepancy since the surface thermochemical solution assumes that the solid participating in the reactions is fully charred. According to the decomposition kinetics, it takes an infinite amount of time for the composite to decompose to its char state. As a result, to ensure that the thermochemistry data is accurately describing the surface ablation phenomenon, a tolerance in the vicinity of the char density could be implemented with which the solid density is automatically adjusted to the char value once this tolerance has been reached. This method is implemented in CMA, but it adds the additional complication of accounting for this mass when solving the gas phase continuity equation.

VII. Conclusions

A one-dimensional charring ablator thermal response code with a contracting grid scheme has been developed and verified to exhibit second order spatial accuracy for the thermochemical ablation problem. Newton's method for the entire system of equations has been implemented and has also been verified to exhibit second order nonlinear convergence rates for both the mixture energy and gas phase continuity equations. The model has shown good agreement with CMA, but it also includes several improvements in the solution procedure, which include the calculation of time accurate nonlinearities, improved integration of decomposition kinetics, and the prediction of pyrolysis gas flow and pore pressure.

Acknowledgments

The authors would like to thank Dave Kuntz and Don Potter for their involvement in technical discussions. In addition, A. J. Amar would like to thank Basil Hassan for his support throughout the project.

References

[1] Moyer, C. B., and Rindal, R. A., "An Analysis of the Coupled Chemically Reacting Boundary Layer and Charring Ablator, Part II, Finite Difference Solution for the In-Depth Response of Charring Materials Considering Surface Chemical and Energy Balances," NASA CR-1061, June 1968.

[2] Suzuki, T., Sawada, K., Yamada, T., and Inatani, Y., "Thermal Response of Ablative Test Piece in Arc-Heated Wind Tunnel," AIAA Paper 2004-341, January 2004.

[3] Blackwell, B. F., "Numerical Prediction of One-Dimensional Ablation Using a Finite Control Volume Procedure with Exponential Differencing," *Numerical Heat Transfer*, Vol. 14, No. 1, 1988, pp. 17-34.

[4] Blackwell, B. F., and Hogan, R. E., "One-Dimensional Ablation Using Landau Transformation and Finite Control Volume Procedure," *Journal of Thermophysics and Heat Transfer*, Vol. 8, No. 2, 1994, pp. 282-287.

[5] Hogan, R. E., Blackwell, B. F., and Cochran, R. J., "Application of Moving Grid Control Volume Finite Element Method to Ablation Problems," *Journal of Thermophysics and Heat Transfer*, Vol. 10, No. 2, 1996, pp. 312-319.

[6] Suzuki, T., Sawada, K., Yamada, T., and Inatani, Y., "Experimental and Numerical Study of Pyrolysis Gas Pressure in Ablating Test Piece," *Journal of Thermophysics and Heat Transfer*, Vol. 19, No. 3, 2005, pp. 266-272.

[7] Chen, Y. -K., Milos, F. S., "Ablation and Thermal Response Program for Spacecraft Heatshield Analysis," *Journal of Spacecraft and Rockets*, Vol. 36, No. 3, 1999, pp. 475-583.

[8] Chen, Y. -K., Milos, F. S., "Two-Dimensional Implicit Thermal Response and Ablation Program for Charring Materials on Hypersonic Space Vehicles," AIAA Paper 2000-0206, January, 2000.

[9] Chen, Y. -K., Milos, F. S., "Three-Dimensional Ablation and Thermal Response Simulation System," AIAA Paper 2005-5064, June, 2005.

[10] Amar, A. J., Blackwell, B.F., Edwards, J. R., "One-Dimensional Ablation with Pyrolysis Gas Flow Using a Full Newton's Method and Finite Control Volume Procedure," AIAA Paper 2006-2910, June 2006.

[11] Amar, A. J., "Modeling of One-Dimensional Ablation with Porous Flow Using Finite Control Volume Procedure," Masters Thesis at North Carolina State University, 2006.